Original Research

Extracellular vesicles extracted from bone marrow mesenchymal stem cells carrying MicroRNA-342-3p inhibit the INHBA/IL13Rα2 axis to suppress the growth and metastasis of breast cancer

Qi Liu [a], Jing Zhang [b], Yi Liu [c], Hai Peng [d], Yingqi Wu [a],[*]

[a] *Department of Breast Surgery, Chifeng Municipal Hospital, No. 1, Middle Section of Zhaowuda Road, Hongshan District, Chifeng 024000, P R China*
[b] *Department of Emergency Medicine, Chifeng Municipal Hospital, Chifeng 024000, P R China*
[c] *Department of Inpatient Pharmacy, Chifeng Municipal Hospital, Chifeng 024000, P R China*
[d] *Department of Oncology, Chifeng Municipal Hospital, Chifeng 024000, P R China*

ABSTRACT

Increasing focus has come to the role of extracellular vesicles (EVs) in various cancers. Hence, we designed this study to explore the mechanism whereby microRNA-342-3p (miR-342-3p)-containing EVs derived from BMSCs might affect breast cancer. MCF-7 breast cancer cell line was co-incubated with the EVs isolated from rat BMSCs, followed by alteration of miR-342-3p and INHBA expression. Microarray-based analyses predicted a possible regulatory mechanism involving miR-342-3p, INHBA, and IL13Rα2 in breast cancer, which was verified by luciferase reporter, RNA pull-down, and RIP assays. Besides, in order to evaluate the effects of miR-342-3p on the biological features of breast cancer cells *in vitro* and *in vivo*, we employed the scratch assay, Transwell assay, CCK-8 assay, and nude mouse tumorigenicity assay. miR-342-3p carried by BMSC-EVs was transferred into breast cancer cells through co-culture, which inhibited the proliferation and metastasis of breast cancer cells *in vitro*. miR-342-3p downregulated the expression of INHBA, which further repressed the expression of IL13Rα2. Finally, the *in vivo* experimental results revealed the inhibitory role of miR-342-3p in tumor growth and metastasis in nude mice. To sum up, BMSC-EVs carrying miR-342-3p could prevent breast cancer growth and metastasis by downregulating the INHBA/IL13Rα2 axis, highlighting a potential target for anti-cancer treatment for breast cancer.

Introduction

Breast cancer is often diagnosed in an advanced and metastatic stage despite campaigns to encourage regular self-inspection and clinical examination of the breast [1, 2]. Treatment strategies for breast cancer vary according to molecular subtype, including locoregional (radiation therapy and surgery) and systemic therapy (endocrine therapy, chemotherapy, bone stabilizing agents, and immunotherapy) approaches [3]. Although survival rate has risen in nearly every type of breast cancer patients, the recurrence rate within five years remains increased among one third of patients and the five-year survival rate in patients with metastasis is lower than 30% [4]. More personalized treatment approaches based on tumor and/or patient molecular profiles is expected to emerge [5]. Hence, we designed this study to explore a potentially more efficient and specific therapy for breast cancer

management involving miR-342-3p-containing bone marrow mesenchymal stem cell-extracellular vesicles (BMSC-EVs).

EVs are released by a range of cells and are recognized as potential biomarkers in normal and pathological conditions due to their participation in cell-cell communication system by delivering a diverse series of biomolecules such as messenger RNAs (mRNAs), microRNAs (miRNAs), proteins, and lipids [6]. A prior study identified EVs as potential biomarkers and therapeutic agents in breast cancer [7]. Besides, there is previous evidence implicating mesenchymal stem cells (MSCs) in tumor progression partly through their secretome [8]. In addition, MSC-derived EVs have the potential to serve as a therapeutic approach in various diseases and hold promise as an alternate cell-free therapy [9] as they can affect disease outcomes by transferring their bioactive cargos miRNAs to recipient target cells [10]. Meanwhile, there is prior evidence showing that miR-342-3p is an inhibitor of the malignant characteristics

of breast cancer cells [11].

Our preliminary binformatics analysis predicted the presence of miR-342-3p binding sites in the 3'UTR of INHBA mRNA. INHBA is a member of the TGF-β superfamily, which links to various malignancies such as gastric cancer, nasopharyngeal carcinoma, and ovarian cancer [12–14]. More importantly, a previous study validated INHBA as a potential prognostic marker for breast cancer [15]. Another recent study has demonstrated that INHBA depletion can cause downregulation of interleukin-13 receptor alpha 2 (IL13Rα2) expression in metastatic breast cancer cells [16]. IL13Rα2 is a subunit of the transmembrane receptor for interleukin-13 and represents another useful prognostic marker for breast cancer [17]. Hence, we predicted that miR-342-3p shuttled by BMSC-EVs may engage in the progression of breast cancer by altering the downstream INHBA/IL13Rα2 axis. Therefore, we undertook the present study employing bioinformatics prediction and *in vitro* and *in vivo* experimental verification with the aim to test our hypothesis about the action of EVs in breast cancer.

Materials and methods

Bioinformatics analysis

Key miRNAs in breast cancer were identified through existing studies, and the enrichment of key miRNAs in human tissues and various cancer EVs and vesicles were predicted using EVmiRNA database. The expression of key miRNAs in breast cancer was determined through the breast cancer miRNA microarray GSE35412 in the GEO database extracted by R language. The downstream genes of miR-342-3p were predicted using mirDIP (Integrated Score > 0.45), DIANA TOOLS (miTG score > 0.95), RNA22, TargetScan (Cumulative weighted context++ score < -0.25) and miRWalk databases (accessibility < 0.01, au > 0.35, bindingp = 1), and the intersection was taken among these prediction results to identify key genes. The interacting genes of key downstream genes were predicted using GeneMANIA database, followed by a protein interaction network construction. The core degree was calculated to determine the key genes. We next analyzed the TCGA database through the GEPIA database to obtain the expression of MRFAP1 and INHBA in breast cancer to further verify the key genes, and then predicted the binding sites of miRNA and key genes from TargetScan. The downstream targets of key genes were determined through existing literature and the MEM database was applied for analysis and verification of their co-expression relationship.

Isolation and identification of BMSCs

Human BMSCs (HUXMA-01001, Cyagen Biosciences Inc., Suzhou, China) in good growth condition were collected and cultured in RPMI 1640 medium with 10% FBS, 1% penicillin-streptomycin (Gibco, Grand Island, NY), and 1% L-glutamine. Cells were prepared into a single cell suspension of 1×10^6/mL, and then incubated with fluorescently labeled antibodies (BD, Franklin Lakes, NJ): CD44-PerCP, CD73-FTTC, CD90, CD105, CD34-PE, CD11b, CD19-APC, CD45-FTTC and HLA-DR at 4°C for 30 min. The unlabeled antibodies were washed off with PBS, and the expression of the corresponding labeled antigen in the sample was measured with a flow cytometer.

The 3rd generation cells were seeded in 48-well plates (2×10^4 cells/well), (three multiple wells set in each group), and cultured with α-MIEM complete culture medium (400 μL/well; 10% FBS, penicillin, and streptomycin) with 5% CO_2 and saturated humidity at 37°C. After the cells had adhered overnight, the culture medium was aspirated, followed by addition of 400 μL/well of complete medium for adipogenic differentiation (HC-DMEM; 10% FBS, 1×10^6 mol/L dexamethasone, 10 ng/mL insulin, and 0.5 μmol/L IBMX) or 400 μL/well of complete medium for osteogenic differentiation (HC-DMEM; 10% FBS, 10 mmol/L β-glycerol phosphate, 10.7 mol/L dexamethasone, and 0.5 μmol/L phosphorylated vitamin C). The control group used HC-DMEM (10%

FBS). Medium was changed every three days. After one week, Oil Red O staining was performed to observe the degree of adipogenic differentiation of the cells. After two weeks, von Kossa staining and Alcian blue staining were performed to observe the osteogenic differentiation and chondrogenic differentiation abilities of BMSCs, respectively.

Isolation of BMSC-EVs

BMSCs were cultured under appropriate conditions until reaching 80% cell density. The cells continued to culture with 10 mL serum-free medium, and 48 h later, the supernatant was harvested to centrifuge (3000 × g; 15 min). Thereafter, the supernatant was mixed with Exo-Quick exosome precipitation solution (63 μL), and centrifuged (1500 × g for 30 min at 20°C). Following supernatant removal, EV pellet was collected and finally resuspended in 100 μL PBS for subsequent experiments.

TEM

First, 10 μL of the isolated EVs (concentration of about 5×10^{11}/mL) were dropped on carbon-coated copper mesh (300 mesh) and absorbed for 90 s, followed by 4% paraformaldehyde fixation in situ for 20 min. Girds were stained with 1% uranyl acetate liquid for 30 s and observed and photographed using a TEM (Hitachi 7650, Tokyo, Japan).

NTA

All EV samples were diluted in PBS to 1 mL, and vortexed for 1 min after which Nanosight NS300 (Malvern Panalytical, Worcestershire, UK) was employed for concentration measurement. The instrument was set according to the instructions of the NanoSight NS300 user's manual (MAN0541-01-EN-00, 2017).

Cell culture

Breast cancer cell lines including MCF-7, SKBR3, T47D and MDA-MB-231, and human normal breast epithelial cell line of MCF10A were purchased from ATCC (Manassas, VA). They were cultured in RPMI 1640 medium (SP1355; 10% FBS, 100 mg/mL streptomycin and 100 U/mL penicillin) in a 5% CO_2 incubator at 37°C with saturated humidity. The medium was renewed every 1 - 2 days, and subculture was conducted upon 80 - 90% cell confluence.

MCF-7 and BMSCs were trypsinized, centrifuged at 1000 × g for 5 min and resuspended in 3 mL of complete medium. Thereafter, 1 mL of the resuspension solution was collected and diluted 20-fold. The diluted cell suspension was mixed, 10 μL of which was collected and placed under a cell counting plate for counting. MCF-7 and BMSCs were settled in a co-culture chamber with a 0.4 μm pore size at a ratio of 3: 1. MCF-7 cells were settled in the basolateral chamber (approximately 1.2×10^5 cells each), BMSCs were settled in the apical chamber (approximately 4×10^6 cells). The co-culture chamber was placed in 6-well plates for co-cultivation, the apical chamber was added with complete medium with 10% serum, and the basolateral chamber with serum medium 10% exosomes-free FBS. The cells were cultured in this environment for 4 - 5 days. Medium in the apical and basolateral chambers was also replaced every 1 - 2 days. Afterwards, cells were collected.

Cell transfection

The gene-specific overexpression plasmids (FulenGen, Guangzhou, Guangdong, China) or siRNAs (GenePharma, Shanghai, China) were transfected into cells to alter the expression of miR-342-3p or INHBA. miRNA mimics, miRNA inhibitors and their negative controls (mimic-NC or inhibitor-NC) were from GenePharma. Lipofectamine 3000 reagent (L3000008, Invitrogen, Carlsbad, CA) was applied for transient transfection at a final concentration of 100 μM. BMSCs were transfected

with the miR-342-3p mimic, miR-342-3p inhibitors, and their respective NCs through lentivirus packaging. The plasmids required for the lentivirus packaging system were from GeneChem Co., Ltd. (Shanghai, China). MCF-7 cells were transfected with miR-342-3p mimic (3'-UGCCCACGCUAAAGACACACUCU-5', 3'-TCAATCACAGATAGCACCCCT-5'), miR-342-3p inhibitor (3'-UCUCACACAGAAAUCGCACCCGU-5'), sh-INHBA (5'-CCATGTCCATGTTGTACTA-3'), miR-342-3p inhibitor + sh-INHBA and their NCs (mimic-NC [3'-ACGGGTGCGAT TTCTGTGTGAGA-5'], inhibitor-NC [3'-TCTCACACAGAAATCGCA CCCGT-5']) using Lipofectamine 3000 reagent for the corresponding experimental analysis. In order to reduce the toxicity of the transfection reagent to cells, the medium was replaced 6 h after transfection and cellular RNA or protein were extracted 48 h after transfection for analysis.

The transient co-transfection system of HEK293T cells (CBP60439, Cobioer Biosciences, Co., Ltd., Nanjing, Jiangsu, China, cultured in DMEM [11965092, Gibco; 10% FBS, 100 mg/mL streptomycin and 100 U/mL penicillin) was used for lentivirus packaging. After 24 h of the lentiviral packaging, the supernatant was collected, and fresh medium was used for the second collection of the supernatant 24 h later. Then, the above two supernatants were mixed for target cell infection. BMSCs transfected with lentivirus were seeded in 24-well plates (5×10^4 cells/well) and underwent incubation overnight. The uptake of virus particles by cells was enhanced by use of a medium with 500 µL of fresh medium, 500 µL of lentiviral supernatant, and 8 µg of polyacrylamide.

Fluorescence labeling and tracking

EVs were extracted as described above, resuspended in 100 µL PBS, and 50 µL of the mixture were mixed with 0.5 mL of Diluent C (CGLDIL-6 × 10ML, Sigma-Aldrich). The mixture was then mixed with the prediluted PKH67 (4 µL PKH67 with 0.5 mL Diluent C) and left to stand for 4 min. Finally, 1 mL 0.5% BSA was used to terminate staining, and EVs were re-extracted. At the same time, Cy3 miRNA labeling kit (Mirus MIR9500) was used to construct fluorescently labeled miR-342-3p for subsequent experiments.

EVs labeled with the fluorescent dye PKH67 (#UR52303, Umibio, Shanghai, China) were co-cultured with breast cancer cells transfected with miR-342-3p labeled with Cy3 (#MIR 9550, Mirus, Madison, WI, US), and fixed with 4% paraformaldehyde for 20 min, with the surface liquid absorbed. The fluorescence effect was observed under a LSM 5 confocal microscope (Carl Zeiss, Jena, Germany). PKH67 labels presented green fluorescence, and Cy3 labels presented red fluorescence.

RT-qPCR

Total RNA from the cells or tissues after different treatments was extracted, and reverse transcribed into cDNA. RT-qPCR was then conducted. β-actin was taken as the internal control, and fold changes were calculated by the $2^{-\Delta\Delta Ct}$ method. The primers used in this assay are presented in Supplementary Table 1. The primers were all provided by GenePharma.

Western blot analysis

Following total protein extraction from cells or tissues, protein concentration was determined using a BCA assay kit (Thermo Fisher Scientific). Then, 30 µg of total protein was subjected to PAGE, transferred onto a PVDF membrane (Amersham, Little Chalfont, UK) and sealed. Thereafter, the membrane was probed with primary rabbit antibodies overnight at 4°C and then with HRP-labeled secondary antibody goat anti-rabbit (1: 5000, ab6721, Abcam). The membrane was developed with an optical luminometer (GE Healthcare, Little Chalfont, Buckinghamshire, UK), and quantified using Image Pro Plus 6.0 software. Primary antibodies used were as follows: CD63 (1: 1000, ab134045, Abcam, Cambridge, UK), Alix (1 µg/mL, ab76608, Abcam),

TSG101 (1: 1000, ab125011, Abcam), Calnexin (1: 1000, ab22595, Abcam), β-actin (1: 5000, ab8227, Abcam), INHBA (1: 1000, ab128958, Abcam), IL13RA2 (1: 1000, ab55275, Abcam), E-cadherin (1: 1000, ab212059, Abcam), N-cadherin (1: 1000, ab19348, Abcam), Vimentin (1: 1000, ab45939, Abcam).

CCK-8 assay

CCK-8 kit (Dojindo, CAT.CK04, Kumamoto, Japan) was used for this assay. Breast cancer cells after different treatment were seeded on a 96-well plate. Starting at a specific time point, the CCK-8 reagent was incubated at 37°C for 2 h. Thereafter, OD450 values were measured using the Infinite M200 spectrophotometer (Switzerland Tecan).

Flow cytometry

Cells were fixed and incubated. Thereafter, 100 µL of cell suspension was washed twice with PBS, centrifuged, resuspended in 200 µL binding buffer, and mixed with 10 µL Annexin V-FITC and 5 µL PI for 15 min, and then with 300 µL binding buffer. Finally, cell apoptosis was measured by a flow cytometer (an excitation wavelength of 488 nm).

Scratch assay

Breast cancer cells following different treatments were cultured under appropriate conditions. When cell density reached 90%, the plate containing the cells was scratched using the tip of a 200 µL pipette to form a scratch. Photos of cultured cells were taken at 0 and 24 h from the same location to evaluate cell migration.

Transwell assay

A matrigel-coated Transwell chamber was pre-heated to 37°C, and cells are separated and collected after different treatments. Cells were resuspended into a uniform cell suspension containing 1×10^5 cells/mL. The complete medium (20% FBS; 600 µL) was put to the lower chamber, and 200 µL of cell suspension to the upper chamber, and incubated for 48 h. The cells were wiped off, fixed and stained before microscopic observation

Luciferase reporter assay

INHBA 3'-UTR MUT or WT firefly luciferase reporter gene plasmids were constructed, and the constructed firefly luciferase plasmid and the control Renilla luciferase vector were co-transfected into MCF7 and T47D cells with mimic-NC and miR-342-3p mimic plasmids. After 24 h, a luciferase assay kit (E1910, Promega) was applied for luciferase activity detection.

RIP assay

The binding of INHBA and IL13Rα2 protein in MCF7 and T47D cells transfected with sh-NC and sh-INHBA was detected by RIP assay. The cells were resuspended in an equal volume of RIPA lysis buffer (P0013B) and centrifuged. A portion of the cell extract served as Input, and another portion was probed with the antibodies against IL13Rα2 (sc-134363, Santa Cruz) and IgG (ab6789, Abcam, serving as a NC) for co-precipitation. After the sample and the control had formed magnetic bead-antibody-gene complexes, RNAs were isolated using TRIzol reagent (Life Technologies Corporation, Gaithersburg, MD) for RT-qPCR detection of INHBA expression.

RNA pull-down assay

MCF7 and T47D cells were transfected with 50 nM of Bio-probe NC, Bio-INHBA-WT and Bio-INHBA-MUT plasmids respectively. Cells were

incubated with specific cell lysis buffer (P0013B, Beyotime). The cell lysate was probed with M-280 streptavidin magnetic beads (Sigma-Aldrich), followed by IL13Rα2 expression detection by Western blot analysis.

Protein stability analysis

MCF7 or T47D cells were divided into INHBA-MUT, INHBA-WT and Control groups. The cells were treated with CHX (#2112, 50 µg/mL, Cell Signaling Technology, Danvers, MA, US) to inhibit protein synthesis Afterwards, the cells were collected at designated time points (0, 0.5, 1, 2, and 3 h), and the protein was extracted from cells. IL13Rα2 protein expression was analyzed by means of Western blot analysis.

Construction of pulmonary metastasis mice model

Forty-eight female BALB/c nude mice (4-6 weeks; weighing between 16 - 22 g; Laboratory Animal Research Center of the Chinese Academy of Sciences (Shanghai, China) were enrolled in the research. Twenty-four nude mice were taken out and randomly divided into four groups (n = 8): EVs, EVs-mimic-NC and EVs-miR-342-3p mimic. EVs from BMSCs transfected with mimic-NC or miR-342-3p mimic and breast cancer cell co-culture suspension (5×10^6 cells/mL) were injected into the tail vein of mice in the experimental group using a disposable sterile syringe, and then EVs (10 µg) were supplemented into the tail vein of mice every 3 d. Control mice were injected with breast cancer cells via tail vein. After injection, mice were housed in the animal experiment center under standard conditions. At 10 to 14 days, tumor cells may have transferred to the lung. After 4 weeks, nude mice were euthanized. Lung tissues were removed, and lung cancer metastases were observed. The number of lung metastases of mice after different treatments was counted. This study was performed under approval of the Ethics Committee of Chifeng Municipal Hospital.

Xenograft tumors in nude mice

Twenty-four nude mice were included for in vivo experiments and randomly grouped (n = 8): EVs, EVs-mimic-NC and EVs-miR-342-3p mimic. EVs from BMSCs transfected with mimic-NC or miR-342-3p mimic. Breast cancer cell co-culture suspension (5×10^6 cells/mL) were injected subcutaneously in the mouse left shoulder with a disposable sterile syringe. Control mice were subcutaneously injected with untreated breast cancer cells. The volume of the subcutaneous tumor was measured every 4 d, and the length (L) and width (W) were measured with a vernier caliper and the final weight of the resected tumor on an electronic balance. The tumor volume (V) was estimated using the following formula, $V = W^2 \times L \times 0.52$. Tumors were removed and used for subsequent experiments.

H&E staining

The subcutaneous tumor tissue of mice was removed, fixed, and dehydrated, paraffin-embedded, and sectioned (4 µm). Sections were dewaxed, hydrated, stained with hematoxylin (H8070-5g) for 25-30 min and counterstained with eosin (PT001) for 2 min. Thereafter, sections were dehydrated, cleared, and mounted before analysis under a DMM-300D optical microscope.

Statistical analysis

SPSS 21.0 software was used to analyze data with measurement data described as mean ± standard deviation. Statistical significance was evaluated by unpaired *t*-test (two-group data), Tukey-corrected one-way ANOVA (multi-group data) or Bonferroni-corrected repeated measures ANOVA (multi-group data at different time points). $p < 0.05$ or $p < 0.01$ was statistically significant.

Results

BMSC-EVs can be internalized by breast cancer cells

In order to study the effect of BMSC-EVs on breast cancer metastasis, BMSCs were initially cultured. Under an inverted microscope, the cultured BMSCs were observed to be normal and with intact cell membrane (Figure 1A), which proved that the BMSCs cultured *in vitro* were in good condition. Red-stained adipocytes, dark-colored calcium nodules and blue-stained acid mucopolysaccharides were observed, indicating that BMSCs had successfully differentiated into adipocytes, osteoblasts and chondroblasts *in vitro* (Figure 1A). Flow cytometric analysis results uncovered that the mesenchymal lineage markers CD44, CD90, CD73, and CD105 were positive, and hematopoietic and endothelial markers CD34, CD19, CD45, CD11b, and HLA-DR were negative (Supplementary Figure 1).

Next, BMSC-EVs were isolated. Observation results under a TEM showed that the isolated EVs were circular and oval membranous vesicles with disc-shaped structure, with a complete capsule, and basically uniform morphology (Figure 1B). Results of NTA demonstrated that the size of EVs was mainly around 100 nm (Figure 1C). Besides, EVs secreted by BMSCs expressed specific marker proteins CD63, Alix, TSG101, but did not express non-labeled protein Calnexin (Figure 1D). This result suggested that BMSC-EVs were isolated successfully. Subsequently, BMSC-EVs were labeled with PKH67 and incubated with MCF-7 cells. Observation under a confocal microscope revealed that the BMSC-EVs could enter the cytoplasm of MCF-7 cells (Figure 1E). In a word, BMSC-EVs can be internalized by breast cancer cells.

BMSC-EVs carrying miR-342-3p inhibits breast cancer cell malignant phenotype while inducing apoptosis

Analysis on the GSE35412 from the GEO database revealed that miR-342-3p had dramatically low expression in breast cancer samples (Figure 2A), in keeping with results from 8 studies in the miRCancer website. At the same time, we found through EVmiRNA analysis that miR-342-3p was enriched in BMSC-EVs (Figure 2B). Hence, we speculated that BMSC-EVs can affect the function of breast cancer cells by transmitting miR-342-3p. The MCF-7 and T47D cell lines had the lowest expression of miR-342-3p and were selected for follow-up experiments (Figure 2C).

It was observed that BMSC-EVs delivered miR-342-3p into MCF-7 and T47D cells (Figure 2D, Supplementary Figure 2A). To verify the effect of BMSC-EVs delivering miR-342-3p (BMSC-EVs-miR-342-3p) on the function of breast cancer cells, miR-342-3p was overexpressed or knocked down in BMSCs, and then the EVs were isolated. BMSC-EVs were co-cultured with MCF-7 and T47D cells. RT-qPCR results revealed that, following miR-342-3p mimic, miR-342-3p expression was increased in co-cultured cells while it was decreased following miR-342-3p inhibitor (Figure 2E, Supplementary Figure 2B).

In addition, MCF-7 and T47D cells treated with EVs-miR-342-3p mimic exhibited weakened proliferation, migration and invasion yet enhanced apoptosis. Opposite results were noted upon EVs-miR-342-3p inhibitor (Figure 2F-I, Supplementary Figure 2C-F). In addition, over-expression of miR-342-3p promoted the expression of E-cadherin and inhibited that of N-cadherin and Vimentin in MCF-7 and T47D cells. In contrast, treatment with EVs-miR-342-3p inhibitor caused contrasting results (Figure 2J, Supplementary Figure 2G).

Collectively, BMSC-EVs can deliver miR-342-3p to breast cancer cells to inhibit the malignant phenotype of breast cancer cells while inducing their apoptosis.

BMSC-EVs-miR-342-3p down-regulates IL13Rα2 expression by inhibiting INHBA

In order to explore the molecular mechanism of miR-342-3p
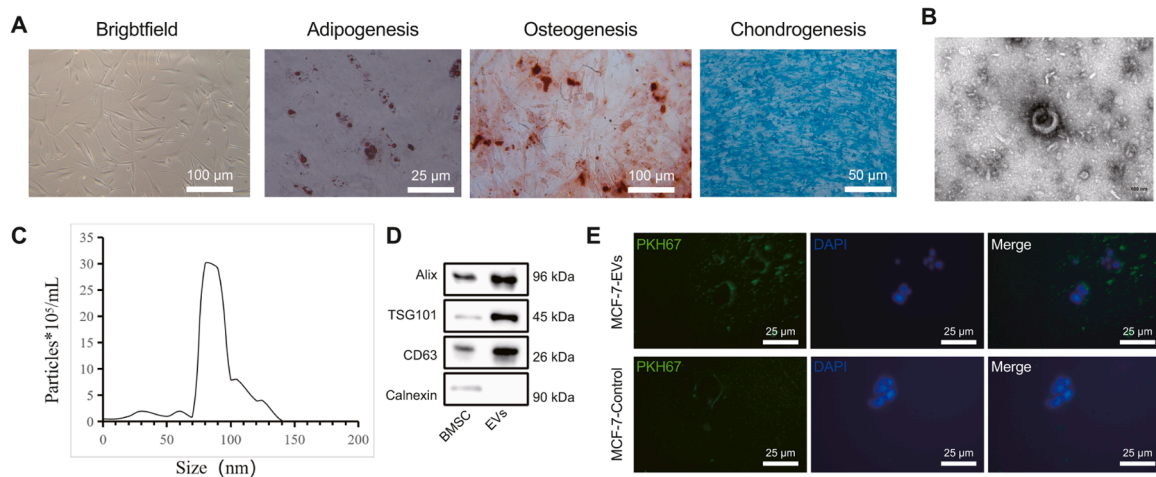
Fig. 1. Breast cancer cells can internalize BMSC-EVs. A, Morphology and adipogenesis, osteogenesis, and chondrogenesis differentiation of BMSC observed under an inverted microscope. B, Morphology of EVs observed under a TEM. C, EV concentration and particle size determined by NTA. D, The expression of EV surface markers Calnexin, Alix, CD63 and TSG101 measured by Western blot analysis (* $p < 0.05$). E, The fluorescent PKH67-labeled BMSC-EVs entering MCF7 cells observed by a confocal microscope. PKH67 labeled EVs are green and DAPI-stained nuclei are blue. All cell experiments were repeated three times.
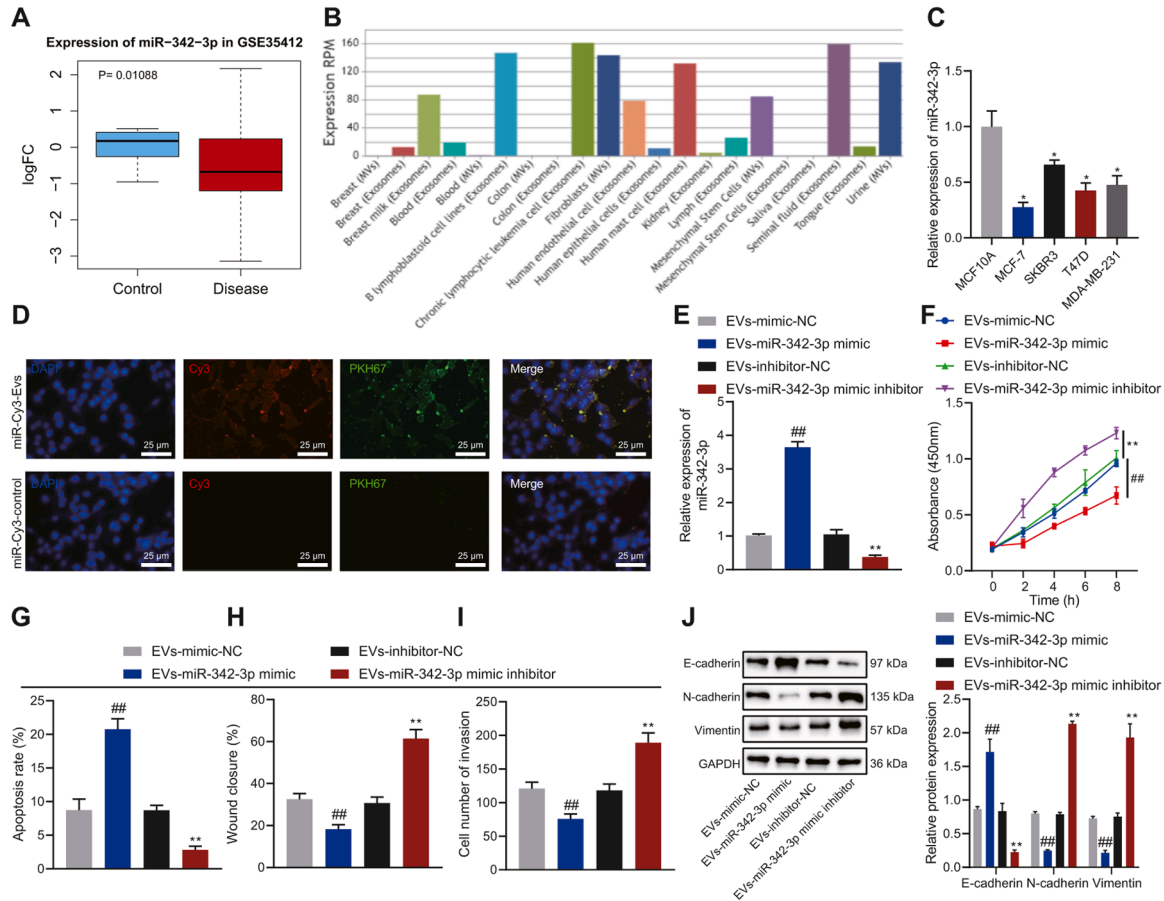
Fig. 2. The effect of BMSC-EVs carrying miR-342-3p on the proliferation, migration, invasion, and apoptosis of MCF-7 cells. A, The expression of miR-342-3p in the microarray GSE35412. B, The enrichment of miR-342-3p in various tissues determined by EVmiRNA. C, The expression of miR-342-3p in breast cancer cells MCF-7, SKBR3, T47D, MDA-MB-231, and human normal breast epithelial cell line MCF10A determined by RT-qPCR, ** $p < 0.01$ in comparison with MCF10A cells. D, The entering of PKH67-labeled EVs carrying Cy3-labeled miR-342-3p into MCF-7 cells observed by a confocal microscope. E, The expression of miR-342-3p in MCF-7 cells incubated with BMSC-EVs determined by RT-qPCR. F, MCF-7 cell proliferation determined by CCK-8 assay. G, MCF-7 cell apoptosis detected by flow cytometry. H, Scratch test of MCF-7 cell migration. I, MCF-7 cell invasion detected by Transwell assay. J, The expression of E-cadherin, N-cadherin and Vimentin in MCF-7 cells determined by Western blot analysis. In panel E-J, ** $p < 0.01$ in comparison with MCF-7 cells incubated with EVs-inhibitor-NC, ## $p < 0.01$ in comparison with MCF-7 cells incubated with EVs-mimic NC. Cell experiments were conducted three times independently.

inhibiting the malignant phenotype of breast cancer, mirDIP, DIANA TOOLS, RNA22, TargetScan and miRWalk databases were employed to predict the downstream genes of miR-342-3p. Results showed that MRFAP1 and INHBA may be the downstream genes of miR-342-3p (Figure 3A). GeneMANIA analysis was then used to predict the top 20 genes in the interaction between MRFAP1 and INHBA, which showed that INHBA (degree = 47) had a higher core degree in the protein interaction network than MRFAP1 (degree = 13) (Figure 3B). The breast cancer data in TCGA database were analyzed by GEPIA and DEGs were screened with $|logFC| > 2$ and $p < 0.05$ as the threshold. INHBA was found to be highly expressed in breast cancer samples, while the expression MRFAP1 showed no obvious difference versus normal samples (Figure 3C, D). INHBA was thus selected for further research.

RT-qPCR results showed highly expressed INHBA in breast cancer cells (Figure 3E). The binding site between miR-342-3p and INHBA was predicted by the TargetScan database. Dual luciferase reporter assay results confirmed that the fluorescence intensity of INHBA 3'UTR-WT was decreased in miR-342-3p mimic-transfected MCF7 and T47D cells while that of INHBA 3'UTR-MUT was not conspicuously altered (Figure 3F, Supplementary Figure 3A).

Based on the results of MEM analysis, INHBA and IL13Rα2 were co-expressed (Figure 3G). The INHBA enrichment by IL13Rα2 was
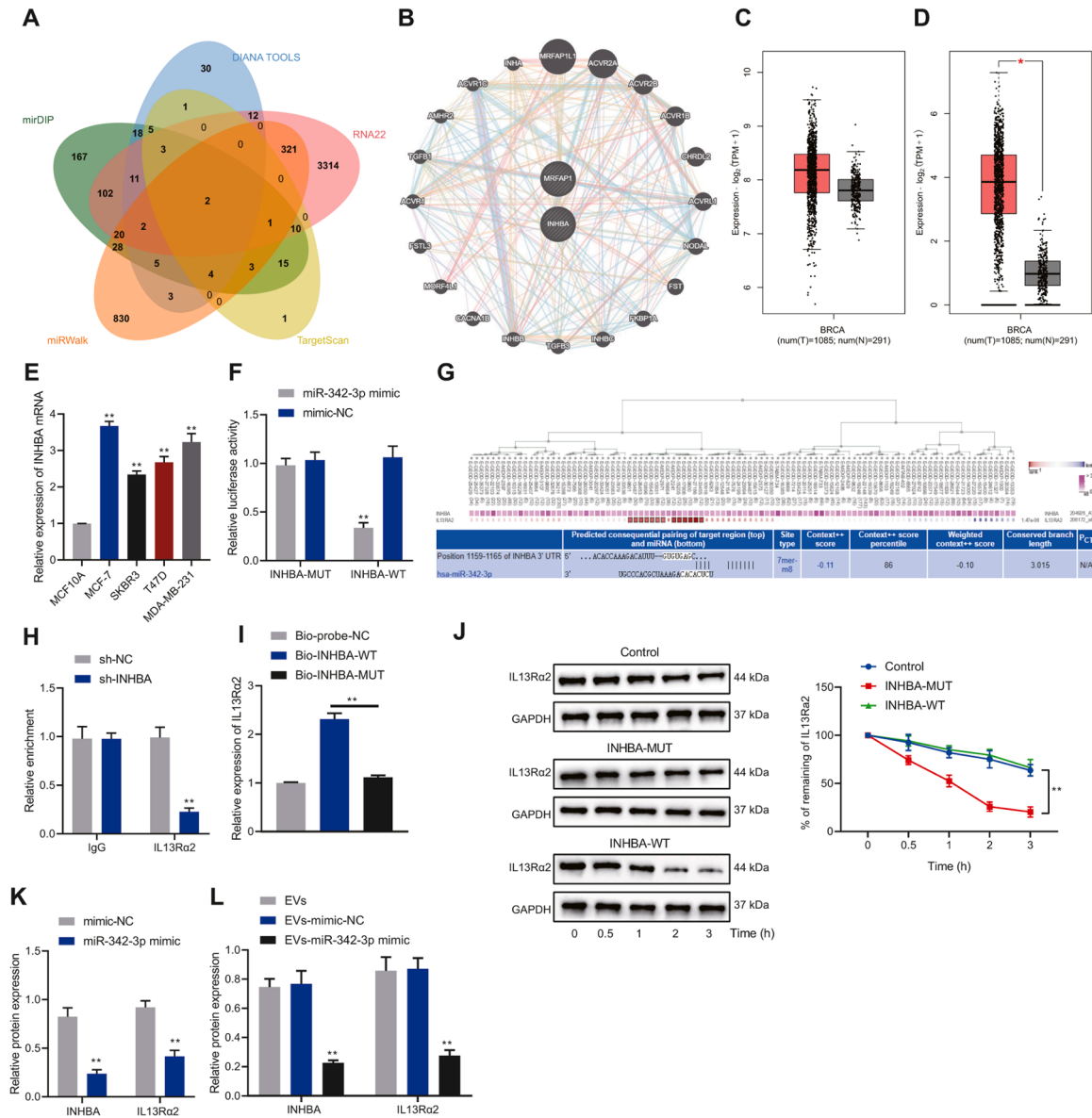
Fig. 3. The effect of BMSC-EVs-miR-342-3p on the expression of INHBA and IL13Rα2 in MCF-7 cells. A, Venn map of miR-342-3p downstream genes predicted by the mirDIP, DIANA TOOLS, RNA22, TargetScan, and miRWalk databases. B, The top 20 genes interacting of MRFAP1 and INHBA predicted by GeneMANIA. C, The expression data of MRFAP1 in breast cancer obtained from the TCGA database analyzed by GEPIA. D, The expression data of INHBA in breast cancer obtained from the TCGA database analyzed by GEPIA, * $p < 0.05$. E, The expression of INHBA in breast cancer cells MCF-7, SKBR3, T47D, MDA-MB-231, and human normal breast epithelial cell line MCF10A measured by RT-qPCR (** $p < 0.01$ in comparison with MCF10A cells). F, The relationship between miR-342-3p and INHBA predicted by TargetScan database and verified by dual luciferase reporter assay in MCF-7 cells, ** $p < 0.01$ in comparison with mimic-NC. G, The relationship between INHBA and IL13Rα2 detected by MEM analysis. H, Binding between INHBA and IL13Rα2 in MCF7 assessed by RIP. ** $p < 0.01$ in comparison with MCF7 cells treated with sh-NC. I, IL13Rα2 protein pulled down by INHBA in MCF-7 cells detected by RNA pull-down assay. ** $p < 0.01$. J, The stability of IL13Rα2 protein in MCF7 cells detected by Western blot analysis. * $p < 0.01$ in comparison with Control MCF7 cells. K, The expression of INHBA and IL13Rα2 in MCF7 cells determined by Western blot analysis, ** $p < 0.01$ in comparison with MCF7 cells transfected with mimic-NC. L, The expression of INHBA and IL13Rα2 in MCF7 cells determined by Western blot analysis, ** $p < 0.01$ in comparison with MCF7 cells treated with EVs-mimic-NC. Cell experiments were conducted three times independently.

significantly reduced in MCF7 and T47D cells transfected with sh-INHBA (Figure 3H, Supplementary Figure 3B). Furthermore, compared with Bio-probe NC and Bio-INHBA-MUT, the treatment of MCF7 and T47D cells with Bio-INHBA-WT pulled down more IL13Rα2 protein (Figure 3I, Supplementary Figure 3C), indicating that INHBA can bind to IL13Rα2 protein. In addition, detection results on the stability of IL13Rα2 protein illustrated that INHBA increased the half-life of IL13Rα2 and increased the stability of IL13Rα2 protein (Figure 3J, Supplementary Figure 3D).

The results of Western blot analysis revealed a decline in the expression of INHBA and IL13Rα2 in MCF7 and T47D cells over-expressing miR-342-3p (Figure 3K, Supplementary Figure 3E). Meanwhile, MCF7 and T47D cells treated with EVs and EVs-mimic-NC showed no alterations in the expression of INHBA and IL13Rα2. Treatment with EVs-miR-342-3p mimic led to a reduction in the expression of INHBA and IL13Rα2 (Figure 3L, Supplementary Figure 3F). Overall, miR-342-3p delivered by BMSC-EVs can downregulate IL13Rα2 expression by inhibiting INHBA.

MiR-342-3p inhibits the malignant phenotype of breast cancer cells while inducing their apoptosis by disrupting the INHBA/IL13Rα2 axis

Next, we intended to elucidate the role of miR-342-3p in the function of MCF7 and T47D cells by regulating the INHBA/IL13Rα2 axis. Transfection of miR-342-3p inhibitor elevated the expression of INHBA and IL13Rα2 in MCF7 and T47D cells, while transfection of sh-INHBA inhibited the expression of INHBA and IL13Rα2 (Figure 4A, Supplementary Figure 4A). Moreover, inhibition of miR-342-3p led to promotion in the migration, proliferation, and invasion of MCF7 and T47D cells, while reducing cell apoptosis. However, inhibition of INHBA reversed these effects of miR-342-3p inhibitor (Figure 4B-E, Supplementary Figure 4B-E).

Moreover, E-cadherin expression was declined, but Vimentin and N-cadherin were elevated in MCF7 and T47D cells with miR-342-3p inhibitor. Conversely, transfection with sh-INHBA undermined effects of miR-342-3p inhibitor (Figure 4F, Supplementary Figure 4F). In short,

miR-342-3p decreased the expression of IL13Rα2 by inhibiting INHBA, thereby suppressing the malignant phenotype of breast cancer cells, while inducing cell apoptosis.

BMSC-EVs-miR-342-3p inhibits the malignant phenotype of breast cancer cells while inducing their apoptosis by disrupting the INHBA/IL13Rα2 axis

The effect of BMSC-EVs-miR-342-3p regulating the INHBA/IL13Rα2 axis on the biological functions of MCF7 and T47D cells was our next focus. INHBA and IL13Rα2 mRNA expression was elevated in MCF7 and T47D cells treated with oe-INHBA + EVs-miR-342-3p mimic (Figure 5A, B, Supplementary Figure 5A, B).

The proliferation, migration, and invasion of MCF7 and T47D cells treated with oe-INHBA + EVs-miR-342-3p mimic were promoted but their apoptosis was inhibited (Figure 5C-F, Supplementary Figure 5C-F). At the same time, Western blot analysis results showed decreased E-cadherin expression yet increased Vimentin and N-cadherin expression in MCF7 and T47D cells treated with oe-INHBA + EVs-miR-342-3p mimic (Figure 5G, Supplementary Figure 5G). To sum up, BMSC-EVs-miR-342-3p repressed the INHBA/IL13Rα2 axis to suppress the malignant phenotype of breast cancer cells while stimulating cell apoptosis.

BMSC-EVs-miR-342-3p inhibits the tumorigenesis and metastasis of cancer cells by disrupting the INHBA/IL13Rα2 axis in vivo

No difference was noted in the tumor volume and weight in mice injected with MCF7 cells treated with EVs and EVs-mimic-NC. Tumor volume and weight were observed to be lower in mice treated with EVs-miR-342-3p than those in mice injected with MCF7 cells treated with EVs-mimic-NC (Figure 6A). No changes were detected in the expression of miR-342-3p, INHBA and IL13Rα2 following treatment with EVs or EVs-mimic-NC. In addition, miR-342-3p expression was augmented, while INHBA and IL13Rα2 expression was reduced, in tumor tissues of EVs-miR-342-3p mimic-treated mice (Figure 6B, C). H&E staining data suggested no difference in the number of lung metastatic nodules in
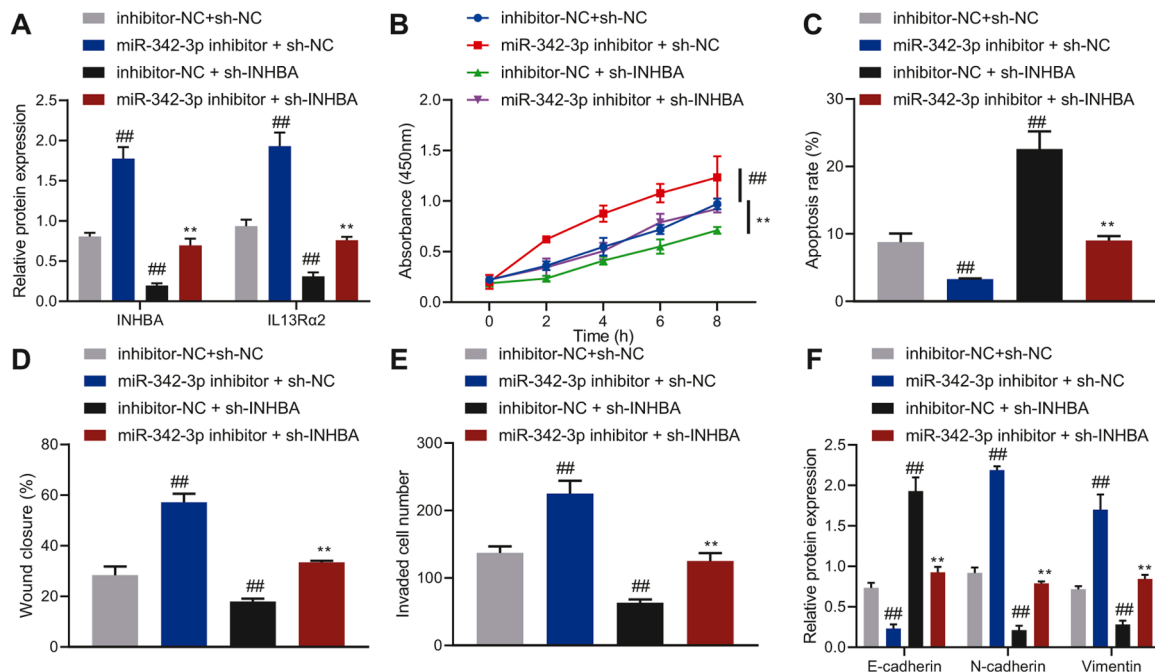
Fig. 4. The effect of miR-342-3p regulating the INHBA/IL13Rα2 axis on the proliferation, migration, invasion and apoptosis of MCF-7 cells. A, The expression of INHBA and IL13Rα2 in MCF-7 cells determined by Western blot analysis. B, MCF-7 cell proliferation determined by CCK-8 assay. C, MCF-7 cell apoptosis determined by flow cytometry. D, MCF-7 cell migration detected by scratch assay. E, MCF-7 cell invasion detected by Transwell assay. F, The expression of E-cadherin, N-cadherin, and Vimentin in MCF-7 cells determined by Western blot analysis, $\#\# p < 0.01$ in comparison with MCF-7 cells transfected with inhibitor-NC + sh-NC, $** p < 0.01$ compared with MCF-7 cells transfected with miR-342-3p inhibitor + sh-NC. Cell experiments were conducted three times independently.
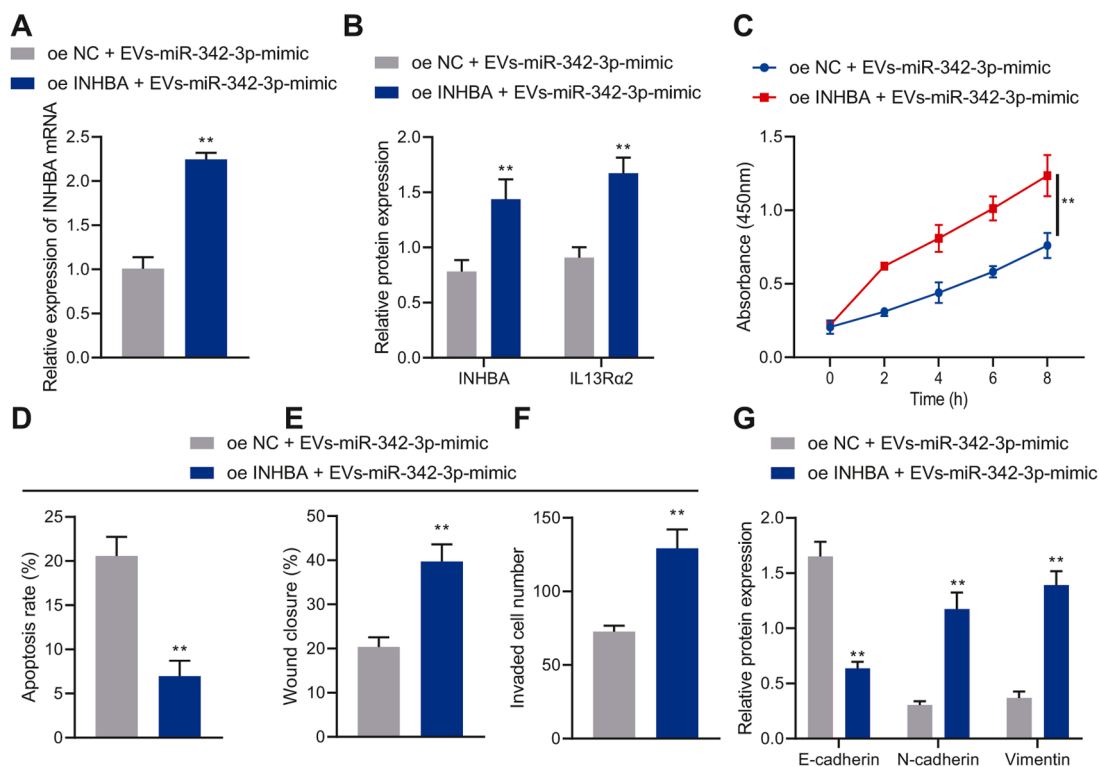
Fig. 5. The effect of BMSC-EVs-miR-342-3p regulating the INHBA/IL13Rα2 axis on the proliferation, migration, invasion, and apoptosis of MCF-7 cells. A, The expression of INHBA in MCF-7 cells determined by RT-qPCR. B, The expression of INHBA and IL13Rα2 in MCF-7 cells determined by Western blot analysis. C, MCF-7 cell proliferation detected by CCK-8 assay. D, MCF-7 cell apoptosis detected by flow cytometry. E, MCF-7 cell migration detected by scratch assay. F, MCF-7 cell invasion detected by Transwell assay. G, The expression of E-cadherin, N-cadherin and Vimentin in MCF-7 cells determined by Western blot analysis. ** $p < 0.01$ compared with MCF-7 cells treated with oe-NC + EVs-miR-342-3p mimic. Cell experiments were conducted three times independently.
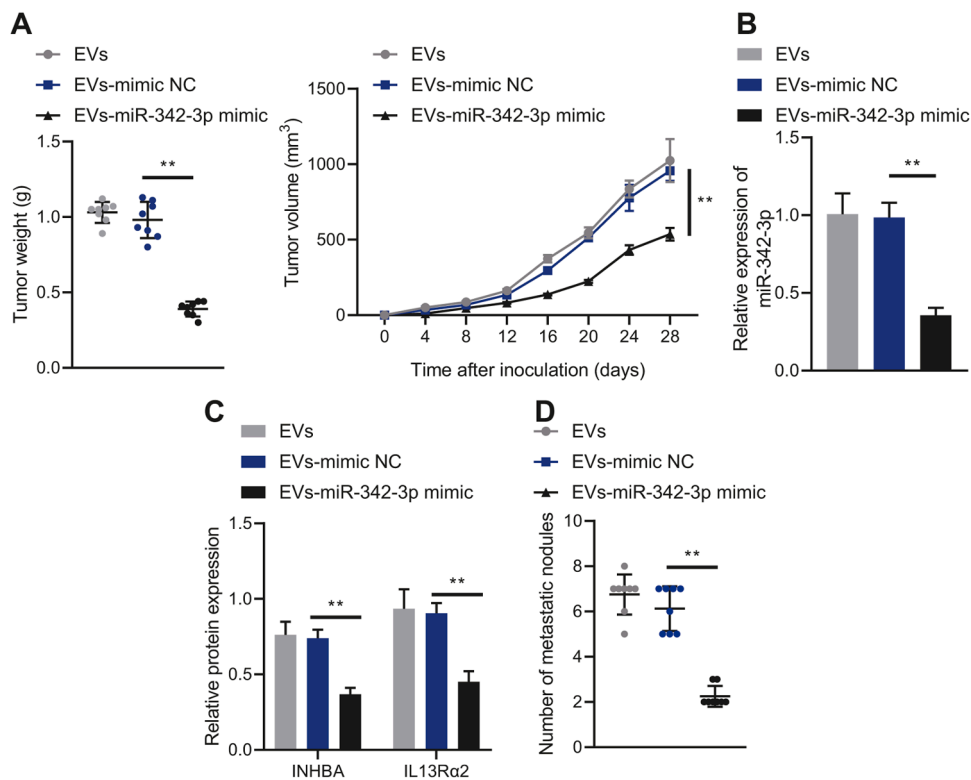
Fig. 6. *In vivo* effect of BMSC-EVs-miR-342-3p regulating the INHBA/IL13Rα2 axis on the tumorigenesis and metastasis of breast cancer. A, Weight and volume of subcutaneously transplanted tumors in nude mice. B, The expression of miR-342-3p in tumor tissues of mice determined by RT-qPCR. C, Protein levels of INHBA and IL13Rα2 in tumor tissues of mice determined by Western blot analysis. D, Lung metastatic nodules observed by H&E staining. n = 8, ** $p < 0.01$.

mice treated with EVs and EVs-mimic-NC. Fewer lung metastasis nodules were observed upon treatment with EVs-miR-342-3p than with EVs-mimic-NC treatment alone (Figure 6D). Cumulatively, BMSC-EVs-miR-342-3p could inhibit the growth and metastasis of cancer cells by downregulating the INHBA/IL13Rα2 axis *in vivo*.

Discussion

In recent years, exosomes derived from BMSCs have been suggested to serve as mediators in breast cancer by delivering miRNAs [18]. Therefore, our study sought to dissect out the effect of BMSC-EVs containing miR-342-3p on breast cancer development. The present study results revealed that BMSC-derived EV miR-342-3p can repress the malignant phenotype of cancer cells by downregulating INHBA-repressed IL13Rα2 to curb breast cancer progression *in vitro* and *in vivo*.

It was initially confirmed that EVs extracted from BMSCs can enter breast cancer cells and repress their malignant phenotype by delivering miR-342-3p. As demonstrated in a previous study, MSC-derived EVs can suppress cell proliferation and enhance adhesion in breast cancer [19]. Interestingly, a prior study elucidated that most exosomal miRs act as either tumor promoters or suppressors after they were internalized into their intracellular target [20]. For instance, EV-packaged miRNAs such as miR-548b-5p and miR-376b-5p are positively related with the survival of breast cancer patients, while miR-375 and miR-24-2-5p were predictive of clinical deterioration [21]. Besides, exosomal miR-342-5p was identified as a novel diagnostic biomarker for the early-stage lung cancer [22], whereas miR-342 in exosomes was a tumor suppressor in breast cancer, which was enhanced by docosahexaenoic acid [23]. These findings testify that EV-carried miR-342-3p from BMSCs could repress the malignant phenotype of cancer cells in breast cancer.

Subsequently, miR-342-3p in BMSC-EVs inhibited the malignant phenotype of breast cancer cells *in vitro* and repressed tumor growth *in vivo* by reducing IL13Rα2 through the downregulation of INHBA. Consistently, a previous study also observed that INHBA silencing arrested the invasion and proliferation of nasopharyngeal carcinoma cells [24]. Likewise, cell migration, invasion, proliferation, and tumor growth were sharply dampened in gastric cancer in response to INHBA knockdown [25]. Moreover, INHBA is down-regulated by miR-376c-3p and thus further mediates the metastatic capability of head and neck squamous cell carcinoma cells [26]. IL13Rα2 is a high-affinity receptor for IL-13 that is recognized as a vital mediator for tumor growth, invasion, and metastasis of diverse human malignancies [27]. For instance, depletion of IL13Rα2 in lung cancer cells hinders invasion *in vitro* and lung metastasis *in vivo*, representing a promising therapy for lung cancer treatment [28]. Further, IL13Rα2 downregulation in metastatic breast cancer cells impedes tumor growth and represses lung metastasis in breast cancer [29]. More importantly, INHBA depletion downregulates IL13Rα2 expression in metastatic breast cancer cells, thus delaying primary tumor growth, suppressing migration *in vitro* and inhibiting the formation of lung metastases *in vivo* [16]. Considering the aforementioned findings, it can be inferred that downregulation of IL13Rα2 induced by miR-342-3p-repressed INHBA in BMSC-EVs acted as a suppressor of breast cancer progression.

Conclusions

The current study proved that BMSC-EVs-miR-342-3p can downregulate IL13Rα2 expression and repress the INHBA/IL13Rα2 axis, thereby inhibiting the growth and metastasis of breast cancer (Figure 7). The accessibility of EV-carried miRs may be an interesting and significant topic for future research topic. We foresee considerable potential for therapeutic strategies directed towards BMSC-EVs-miR-342-3p.

Funding

Availability of data and material

The data that support the findings of this study are available from the corresponding author upon reasonable request.

Author Contributions

Qi Liu and Hai Peng designed the study. Jing Zhang and Yingqi Wu collated the data, carried out data analyses and produced the initial draft of the manuscript. Qi Liu and Yi Liu contributed to drafting the manuscript. All authors have read and approved the final submitted manuscript.
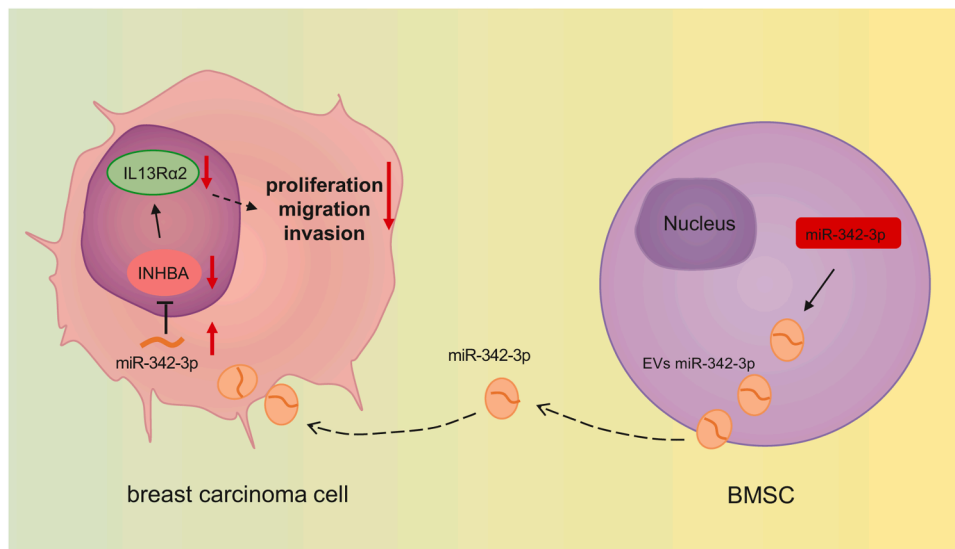
Fig. 7. Schematic diagram of the mechanism by which BMSC-EVs carrying miR-342-3p affect the growth and metastasis of breast cancer. BMSC-EVs carrying miR-342-3p to breast cancer cells, where miR-342-3p downregulated the expression of INHBA and IL13Rα2 and repressed breast cancer cell proliferation, migration, and invasion while inducing cell apoptosis, thus preventing the growth and metastasis of breast cancer.

Declaration of Competing Interest

None.

Supplementary materials

Supplementary material associated with this article can be found, in the online version, at doi:10.1016/j.tranon.2021.101333.

References

[1] M. Akram, S.A. Siddiqui, Breast cancer management: past, present and evolving, Indian J. Cancer 49 (3) (2012) 277–282.

[2] M. Akram, M. Iqbal, M. Daniyal, A.U. Khan, Awareness and current knowledge of breast cancer, Biol. Res. 50 (1) (2017) 33.

[3] N. Harbeck, F. Penault-Llorca, J. Cortes, M. Gnant, N. Houssami, P. Poortmans, et al., Breast cancer, Nat. Rev. Dis. Primers 5 (1) (2019) 66.

[4] X. Wu, A.B. Shaikh, Y. Yu, Y. Li, S. Ni, A. Lu, et al., Potential diagnostic and therapeutic applications of oligonucleotide aptamers in breast cancer, Int. J. Mol. Sci. 18 (9) (2017) 1851.

[5] R. Sabatier, A. Goncalves, F. Bertucci, Personalized medicine: present and future of breast cancer management, Crit. Rev. Oncol. Hematol. 91 (3) (2014) 223–233.

[6] F.S.Y. Yoshikawa, F.M.E. Teixeira, M.N. Sato, L. Oliveira, Delivery of microRNAs by extracellular vesicles in viral infections: could the news be packaged? Cells 8 (6) (2019) 611.

[7] R.J. Mo, J.M. Lu, Y.P. Wan, W. Hua, Y.X. Liang, Y.J. Zhuo, et al., Decreased HoxD10 expression promotes a proliferative and aggressive phenotype in prostate cancer, Curr. Mol. Med. 17 (1) (2017) 70–78.

[8] X. Zhou, T. Li, Y. Chen, N. Zhang, P. Wang, Y. Liang, et al., Mesenchymal stem cellderived extracellular vesicles promote the in vitro proliferation and migration of breast cancer cells through the activation of the ERK pathway, Int. J. Oncol. 54 (5) (2019) 1843–1852.

[9] S. Rani, A.E. Ryan, M.D. Griffin, T. Ritter, Mesenchymal stem cell-derived extracellular vesicles: toward cell-free therapeutic applications, Mol. Ther. 23 (5) (2015) 812–823.

[10] G. Qiu, G. Zheng, M. Ge, J. Wang, R. Huang, Q. Shu, et al., Mesenchymal stem cell-derived extracellular vesicles affect disease outcomes via transfer of microRNAs, Stem Cell Res. Ther 9 (1) (2018) 320.

[11] C. Liu, H. Xing, X. Luo, Y. Wang, MicroRNA-342 targets Cofilin 1 to suppress the growth, migration and invasion of human breast cancer cells, Arch. Biochem. Biophys. 687 (2020), 108385.

[12] C. Zhang, Y. Liang, M.H. Ma, K.Z. Wu, D.Q. Dai, KRT15, INHBA, MATN3, and AGT are aberrantly methylated and differentially expressed in gastric cancer and associated with prognosis, Pathol. Res. Pract. 215 (5) (2019) 893–899.

[13] S. Lyu, C. Jiang, R. Xu, Y. Huang, S. Yan, INHBA upregulation correlates with poorer prognosis in patients with esophageal squamous cell carcinoma, Cancer Manag. Res. 10 (2018) 1585–1596.

[14] X. Li, Z. Yang, S. Xu, Z. Wang, P. Jin, X. Yang, et al., Targeting INHBA in ovarian cancer cells suppresses cancer xenograft growth by attenuating stromal fibroblast activation, Dis. Markers (2019), 7275289 (2019).

[15] Y. Liu, P.R. Pandey, S. Sharma, F. Xing, K. Wu, A. Chittiboyina, et al., ID2 and GJB2 promote early-stage breast cancer progression by regulating cancer stemness, Breast Cancer Res. Treat. 175 (1) (2019) 77–90.

[16] M. Kalli, F. Mpekris, C.K. Wong, M. Panagi, S. Ozturk, S. Thiagalingam, et al., Activin A signaling regulates IL13Ralpha2 expression to promote breast cancer metastasis, Front. Oncol. 9 (2019) 32.

[17] H.J. Kwon, J.E. Choi, Y.K. Bae, Interleukin-13 receptor alpha 2 expression in tumor cells is associated with reduced disease-free survival in patients with luminal subtype invasive breast cancer, Tumour Biol. 40 (6) (2018), 1010428318783657.

[18] Z. Naseri, R.K. Oskuee, M.R. Jaafari, M.Forouzandeh Moghadam, Exosome-mediated delivery of functionally active miRNA-142-3p inhibitor reduces tumorigenicity of breast cancer in vitro and in vivo, Int. J. Nanomed. 13 (2018) 7727–7747.

[19] J. Casson, O.G. Davies, C.A. Smith, M.J. Dalby, C.C. Berry, Mesenchymal stem cell-derived extracellular vesicles may promote breast cancer cell dormancy, J. Tissue Eng. 9 (2018), 2041731418810093.

[20] Q. Liu, F. Peng, J. Chen, The role of exosomal MicroRNAs in the tumor microenvironment of breast cancer, Int. J. Mol. Sci. 20 (16) (2019) 3884.

[21] C. Yan, J. Hu, Y. Yang, H. Hu, D. Zhou, M. Ma, et al., Plasma extracellular vesiclepackaged microRNAs as candidate diagnostic biomarkers for earlystage breast cancer, Mol. Med. Rep. 20 (5) (2019) 3991–4002.

[22] Z. Han, Y. Li, J. Zhang, C. Guo, Q. Li, X. Zhang, et al., Tumor-derived circulating exosomal miR-342-5p and miR-574-5p as promising diagnostic biomarkers for early-stage lung adenocarcinoma, Int. J. Med. Sci. 17 (10) (2020) 1428–1438.

[23] C. Aslan, S. Maralbashi, H. Kahroba, M. Asadi, M.S. Soltani-Zangbar, M. Javadian, et al., Docosahexaenoic acid (DHA) inhibits pro-angiogenic effects of breast cancer cells via down-regulating cellular and exosomal expression of angiogenic genes and microRNAs, Life Sci. 258 (2020), 118094.

[24] S. Peng, J. Wang, P. Hu, W. Zhang, H. Li, L. Xu, INHBA knockdown inhibits proliferation and invasion of nasopharyngeal carcinoma SUNE1 cells in vitro, Int. J. Clin. Exp. Pathol. 13 (5) (2020) 854–868.

[25] Z.L. Chen, L. Qin, X.B. Peng, Y. Hu, B. Liu, INHBA gene silencing inhibits gastric cancer cell migration and invasion by impeding activation of the TGF-beta signaling pathway, J. Cell. Physiol. 234 (10) (2019) 18065–18074.

[26] W.M. Chang, Y.F. Lin, C.Y. Su, H.Y. Peng, Y.C. Chang, T.C. Lai, et al., Dysregulation of RUNX2/activin-A axis upon miR-376c downregulation promotes lymph node metastasis in head and neck squamous cell carcinoma, Cancer Res. 76 (24) (2016) 7140–7150.

[27] Z. Zhao, L. Wang, W. Xu, IL-13Ralpha2 mediates PNR-induced migration and metastasis in ERalpha-negative breast cancer, Oncogene 34 (12) (2015) 1596–1607.

[28] M. Xie, X.J. Wu, J.J. Zhang, C.S. He, IL-13 receptor alpha2 is a negative prognostic factor in human lung cancer and stimulates lung cancer growth in mice, Oncotarget 6 (32) (2015) 32902–32913.

[29] P. Papageorgis, S. Ozturk, A.W. Lambert, C.M. Neophytou, A. Tzatsos, C.K. Wong, et al., Targeting IL13Ralpha2 activates STAT6-TP63 pathway to suppress breast cancer lung metastasis, Breast Cancer Res. 17 (2015) 98.